Photoconductivity in CdSe quantum dot solids

C. A. Leatherdale, C. R. Kagan,* N. Y. Morgan, S. A. Empedocles,† M. A. Kastner, and M. G. Bawendi‡
Chemistry Department, Physics Department, and Center for Materials Science and Engineering, Massachusetts Institute of Technology, 77 Massachusetts Avenue, Cambridge, Massachusetts 02139
(Received 8 February 2000; revised manuscript received 21 April 2000)

We report measurements of photoconductivity and electric field induced photoluminescence quenching in three-dimensional close-packed solids of colloidal CdSe quantum dots. Our measurements suggest that photoexcited, quantum confined excitons are ionized by the applied electric field with a rate that depends on both the size and surface passivation of the quantum dots. Separation of electron-hole pairs confined to the core of the quantum dot requires significantly more energy than separation of carriers trapped at the surface and occurs through tunneling processes. We present a simple resonant tunneling model for the initial charge separation step that qualitatively reproduces both the size and surface dependence of the photoconductivity as a function of applied field. We show that the charge generation efficiency increases with increasing temperature as nonradiative and radiative recombination pathways increasingly compete with charge separation.

I. INTRODUCTION

Two- and three-dimensional arrays of quantum dots (QD's) are of interest both as model ''artificial solids'' with potentially tunable optical and electronic properties[1] and as materials for possible applications in memory[2] and computation.[3–5] Colloidal nanocrystals are promising ''building blocks'' for fabricating such materials as these ''artificial atoms'' exhibit size dependent, atomic-like energy states[6,7] and self-assemble into both glassy and crystalline close-packed solids.[8–10] In principle, interparticle couplings in QD arrays could be engineered by modifying the size and chemistry of the QDs as well as the length and electronic structure of the surface ligands. Promising results have already been achieved with metal colloidal nanocrystals[11,12] including demonstration of a reversible metal-Mott insulator transition as a monolayer of Ag nanocrystals was compressed on a Langmuir trough.[13]

Semiconductor quantum dot arrays, in contrast to their metallic counterparts, offer the possibility of investigating transport in an artificial solid in the limits of strong quantum confinement and weak dielectric screening. While early work has shown that quantum-mechanical coupling between adjacent semiconductor QDs is weak and excitations are largely confined to individual QDs,[14,15] long-range Coulomb interactions between charge carriers are expected to play a significant role in the transport properties.[16] Semiconductor QDs also have potential uses in a variety of optoelectronic devices including light emitting diodes,[17–19] photodetectors,[20,21] and photovoltaic cells.[22,23] Since the emission and absorption characteristics of a semiconductor QD depend on its size, the emission color and spectral response of these devices are tunable. A basic understanding of how charges are captured by and escape from a charge neutral QD, as well as the process of charge separation of a photogenerated excitation created within a QD, is essential for the rational design of these optoelectronic devices.

Photoconductivity is a valuable tool to probe charge separation, charge trapping, and carrier recombination mechanisms in materials. In this paper, we present steady state photoconductivity and fluorescence quenching measurements on close-packed glassy solids of colloidal CdSe QDs. In Sec. III, the dependence of the photoconductivity on temperature, applied electric field, excitation energy, intensity, QD radius interparticle separation, and surface passivation is briefly presented. In Secs. IV A–IV E, we discuss these results in detail and show that photoconductivity in QD solids is consistent with electric field ionization of photoexcited, quantum confined electron-hole pairs. Similar to photoconductivity in many other molecular-like systems, the charge generation efficiency depends on the rate of charge separation relative to the rate of geminate recombination of the photoexcited electron-hole pair. In Sec. IV F, a simple resonant tunneling model is presented to describe the probability of electron-hole pair separation as a function of applied electric field. We show that the energy required for charge separation in QD solids is much greater than kT at room temperature. Thus although most of the experiments described in this paper are performed at 10 K, the results are applicable to room temperature operation of the photovoltaic devices and light emitting diodes currently under study.

II. EXPERIMENTAL DETAILS

A. Sample preparation

The preparation and structural characterization of glassy films of colloidal CdSe QDs have been described in previous publications.[8,15] However, because the method of sample preparation is critical for obtaining conducting solids and consistent surface passivation, we briefly reiterate our methods:

Following the method of Murray and co-workers,[24,25] CdSe QDs are prepared by the pyrolysis of organometallic precursors in a hot coordinating solvent of trioctylphosphine (TOP) and trioctylphosphine oxide (TOPO). The TOPO/TOP surface ligands moderate the growth rate of the QDs, electronically passivate the surface of the QD, and sterically stabilize the QDs in solution, preventing irreversible aggregation. The QDs are isolated from their growth solution and size selected by repeated (3×) precipitation from *n*-butanol

dispersion using methanol as the nonsolvent. This process further narrows the size distribution and ensures the removal of excess TOP/TOPO, not bound to the QDs surfaces, that can phase separate and crystallize in the solid. The resulting powder is dried under vacuum and redispersed in a suitable solvent mixture (see below) for drop casting. Tributylphosphine (TBP)/tributylphosphine oxide (TBPO), pyridine, and octanethiol capped QDs are prepared by repeated dispersion and flocculation of the QDs from a neat solution of the new capping group, followed by washing to remove the excess cap once the exchange is complete. Overcoating of bare CdSe QDs with ZnS or CdS is performed using previously described methods.[26,27]

Close-packed solids are drop cast from solution on to lithographically patterned sapphire or silicon substrates (described below). In order to minimize the exposure of the sample to air, all electrical contacts are made *prior* to film deposition. For this report, a 9:1 hexane/octane solution is used for casting glassy films of TOPO/TOP, TBPO/TBP, and octanethiol capped dots. Pyridine capped dots are deposited from a 9:1 methanol and pyridine mixture on Si/SiO_2 substrates that are boiled in ultrapure water and then dried at 175 °C to make the oxide surface more hydrophilic.[28] Scanning electron microscopy reveals that cracks form in the QD solid if it is not allowed to dry sufficiently before exposure to vacuum. In films deposited and allowed to dry in inert atmosphere overnight before testing, the degree of cracking is reduced but the qualitative electrical behavior and photoconductive gain is the same as that measured for films tested immediately after deposition. All samples exhibit band edge photoluminescence (typically 10% quantum yield in the growth solution at room temperature) and minimal deep trap photoluminescence (PL). QD radii and inter-particle spacing are quoted from published small angle x-ray scattering and transmission electron microscopy measurements.[8,24] QD radii in all cases include the surface layer.

Polished sapphire optical flats or degenerately doped silicon substrates with either a 600 nm or 350 nm thermally grown gate oxide, are used as substrates for photoconductivity measurements. Gold bar electrodes ($200\times800\times0.1\,\mu m^3$) with separations varying from 1 to 20 μm are patterned on the substrates using standard photolithographic techniques. Following the patterning process, the substrates are cleaned by O_2 plasma ash to reduce organic surface contamination before deposition of the QD solid.

B. Photoconductivity measurements

All measurements are performed under vacuum in a cold finger cryostat. Typically, dc photoconductivity of the QD solid is recorded while varying the applied field in steps of 10^4 V/cm with a 10 to 30 sec delay after each step to allow the current to settle. A Keithley 6517 electrometer is used to apply a bias voltage and measure current. The excitation source for the photoconductivity experiments is an argon ion laser with typical excitation intensity of $\sim$2.5 mW/cm^2. For measurement of the spectral dependence of the photocurrent, a SPEX Fluorolog-2 spectrofluorimeter with a 450W Hg-Xe arc lamp in combination with a 0.22 m double monochromator is used as the excitation source (intensity$\sim$1 mW/cm^2). The energy dependence of the lamp intensity is accounted for by measuring the emission from a reference cell containing a concentrated dye solution (Rhodamine 610 or 640). The spectral response is further corrected by excitation correction factors created for each of the dyes to account for the $\sim$10% error resulting from the difference in optical path from the positions of the reference dye cell and the sample.

Multiple electrode separations are tested (from 1 to 20 μm); the results depend only on the applied field for samples of different electrode separation, thus eliminating the contacts as a significant source of the circuit resistance. Several experiments are performed to compare the I-V curve when both the active sample area and gold electrodes are illuminated to the I-V curve when only the active sample area is illuminated. Since there are no qualitative differences in the I-V characteristics that might indicate photoinjection from the electrodes, for all subsequent experiments the entire electrode pattern is illuminated. Intensity dependent measurements are acquired in nonsequential order using a neutral density wheel to modify the laser intensity.

C. Optical measurements

To develop a complete picture of the charge generation process, the photoconductivity results are correlated with a variety of optical measurements. To measure the temperature dependence of the PL quantum yield (QY), linear absorption and PL spectra for the films are measured using a 300 W Hg-Xe lamp, SPEX 0.33 m monochromator, and an optical multi-channel analyzer. The PL is excited as before with a low intensity laser beam or with a Hg-Xe lamp plus monochromator combination. Quenching of the fluorescence in an electric field is measured using a far field epifluorescence microscope described elsewhere.[29] The fluorescence image of the electrodes and sample is projected on to the entrance slits of the monochromator, which are then narrowed so that only the emission from the center region between the electrodes is collected. A mode locked Nd:YAG/dye laser system and a time correlated single photon counting apparatus with $\sim$150 ps time resolution is used for PL lifetime measurements.

III. RESULTS

Figure 1 shows the photocurrent spectral response for a representative series of QD sizes. For each sample, the spectral response is scaled to match the lowest energy feature in the linear absorption spectrum. The well resolved, discrete electronic transitions in the absorption spectra demonstrate the monodispersity of the QD samples.[30] The shape of the photocurrent spectral response follows the linear absorption spectrum, independent of applied field and temperature ($T<150$ K). No photocurrent is observed for excitation below the band edge suggesting that optical excitation of charges directly out of sub-bandgap trap states makes a negligible contribution to the photocurrent. The spectral response of the QD solid is clear evidence that free carriers originate from quantum confined electron-hole pairs created within individual QDs.[31,32]

While there is close correspondence between the absorption spectrum and the photocurrent spectral response near the band edge, the spectral response slowly deviates from the

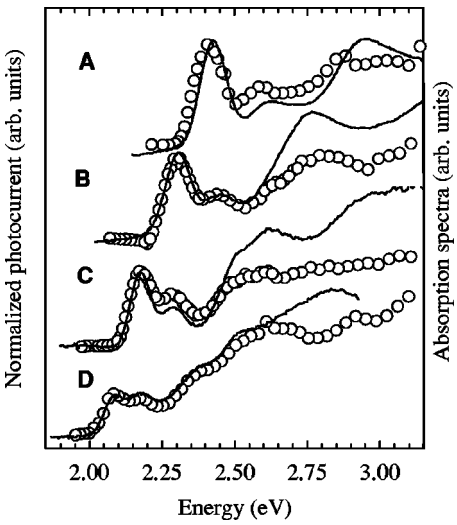

FIG. 1. Spectral dependence of photocurrent at 10 K. The symbols indicate the photocurrent at a fixed applied electric field of 2.5×10^5 V/cm, normalized for excitation intensity. The solid line is the corresponding linear absorption spectrum for each sample. The photocurrent spectral response is scaled to match the first absorption feature. The QDs in each sample have the following radii: *A*—17.5 Å, *B*—20.6 Å, *C*—25 Å, and *D*—30 Å.

absorption spectrum as the excitation energy is increased above the band edge. A similar trend has been previously observed in photoluminescence excitation studies on dilute ensembles of CdSe QDs and is consistent with an increase in the nonradiative recombination rate of the exciton at higher energy excitation. Since excitation with energies well above the band edge does not enhance the charge generation efficiency (number of charges/absorbed photon), charge separation must be a slower process than intraband relaxation to the lowest excited state. This result is not surprising given the fast intra-band relaxation times (<300 fs) reported for colloidal semiconductor QDs.[33]

Figure 2 shows that the photocurrent varies linearly with excitation intensity. Linear dependence is observed over two orders of magnitude in intensity, independent of electrode

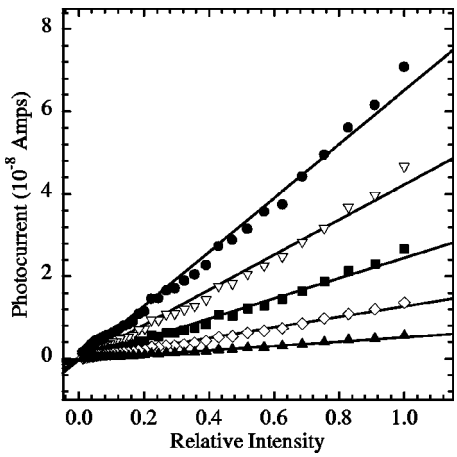

FIG. 2. Intensity dependence of the photocurrent at 10 K for a 21 Å radius QD solid. Symbols are the photocurrent at an applied field of (●) 250 kV/cm, (▽) 200 kV/cm, (■) 150 kV/cm, (◇) 100 kV/cm, and (▲) 50 kV/cm.

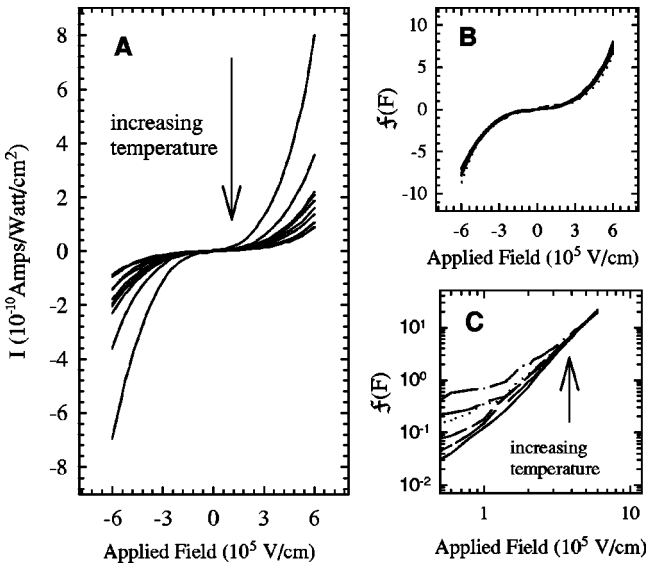

FIG. 3. (a) Temperature dependence of the photocurrent for a 19 Å TBPO/TBP capped QD solid. *I-V* curves are shown for 10, 25, 50, 75, 100, 150, 200, 250, and 293 K. (b) The *I-V* curves from (a) are each multiplied by a scale factor, $S(T)$, to show that they collapse onto a single universal curve, $f(F)$. (c) The *I-V* curves for a 18.5 Å TOPO/TOP capped QD solid at 10, 50, 75, 100, 125, and 300 K [note this is a different sample than the data in (a) and (b)]. Each curve has been multiplied by a scale factor to give the best fit to a single universal curve.

spacing, temperature, applied electric field and excitation energy.[31] The photoconductive gain, even at high fields, is only on the order of 10^{-4} charges/photon. The dark current is approximately two orders of magnitude smaller than the photocurrent and lies below the noise level for the measurement apparatus (<0.1 pA). High sensitivity, dark current measurements will be discussed in a forthcoming publication.[34] In this paper, the total current I is equal to the photocurrent I_{pc}.

The absolute magnitude of the photocurrent decreases with increasing temperature [Fig. 3(a)]. However, the shape of the *I-V* characteristic is nearly independent of temperature. Figure 3(b) shows the same *I-V* curves as in Fig. 3(a), each multiplied by a scaling factor so that they collapse on to a single universal curve, $f(F)$ where F is the applied field. Remarkably, there is virtually no change in the shape of the *I-V* characteristics from 10 to 300 K. Figure 3(b) is one of the best examples of a universal *I-V* curve that we have observed. For other samples, the shape of the *I-V* characteristic is weakly temperature dependent and the curvature of the *I-V* characteristic decreases slightly with increasing temperature [Fig. 3(c)]. No systematic trends with QD size or surface ligands have been identified that affect whether the shape of the *I-V* characteristic is temperature dependent.

Figure 4 compares the temperature dependent scaling factor, $1/S(T)$ [used to scale the *I-V* curves as in Fig. 3(b)], QY(T), and exciton lifetime $\tau(T)$ relative to their values at 10 K. The exciton lifetime, $\tau=1/(k_r+k_{nr})$ where, k_r and k_{nr} are the radiative and nonradiative relaxation rates, is measured for a close-packed film of the same size QDs as used for the photocurrent measurements. Both QY(T) and $\tau(T)$ fall

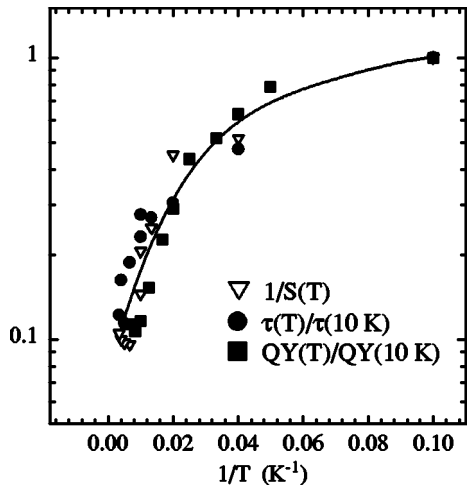

FIG. 4. Temperature dependence of the scale factor $[1/S(T)]$ (∇) from the data in Fig. 3(a) compared to the temperature dependence of the PL lifetime ($\bullet$) and the PL QY ($\blacksquare$), relative to their values at 10 K. Lifetime and QY data is for a 18.2 Å TOPO/TOP capped QD solid.

sharply with increasing temperature, consistent with an increase in the nonradiative rate.

The shape of the *I-V* characteristic depends on QD size. Figure 5 shows *I-V* curves for a series of QD sizes and constant interparticle spacing (TOPO/TOP ligands). As the QD radius decreases, the curvature of the *I-V* curve increases slightly. In order to account for small variations in optical density and excitation intensity and to better examine changes in the shape of the *I-V* characteristics, each *I-V* curve is scaled by a constant factor so that the high field photocurrent is the same for all. Within the signal to noise, the photocurrent rises smoothly with increasing applied electric field, without any inflection points that could indicate the onset of saturation or a clear onset of the photocurrent. No systematic trend in the photoconductive gain as a function of QD size is observed.

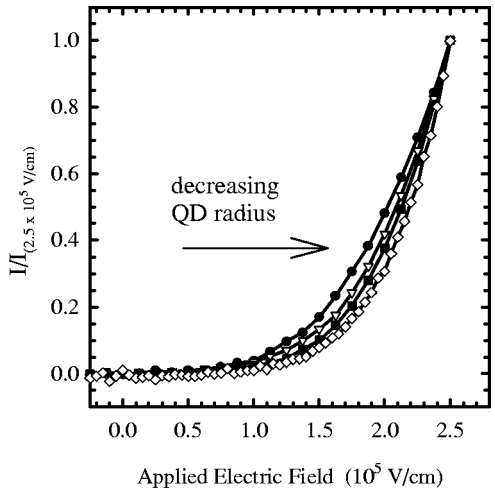

FIG. 5. Current versus applied electric field for QDs with radii(R) as follows: ($\bullet$) 25 Å, (∇) 20.6 Å, ($\blacksquare$) 19 Å, and ($\diamond$) 17.5 Å. Samples are TOPO/TOP capped QDs with edge to edge spacing (d)$\sim$11 Å. Measurements at 10 K. See text for description of the normalization.

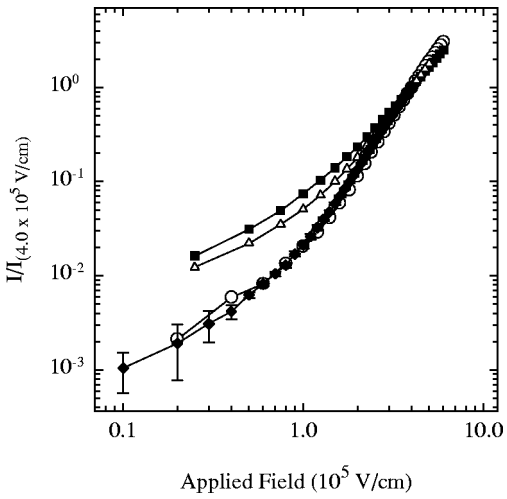

FIG. 6. Effect of the surface ligand on *I-V* curve shape at 10 K for 20$\pm$1 Å QDs with ($\blacklozenge$) TOPO/TOP, ($\triangle$) TBPO/TBP, ($\bigcirc$) octanethiol, and ($\blacksquare$) pyridine ligands. Error bars indicate the approximate variance in the relative positions of each curve based on multiple *I-V* sweeps and multiple samples. Note data is normalized to one at 400 kV/cm.

The *I-V* characteristics depend more strongly on interparticle spacing than surface ligand functionality. Figure 6 shows *I-V* curves where the size of the QD is kept constant and the surface ligand is systematically varied. Exchanging the TOPO linkage (also 8 carbon chains) ($\blacklozenge$) to an octanethiol linkage ($\bigcirc$) does not affect the *I-V* characteristics significantly. Changing to an aromatic while keeping the inter-particle spacing constant [pyridine ($\blacksquare$) vs TBPO ($\triangle$)] also does not affect the *I-V* characteristics significantly. It is clear that QDs passivated with shorter ligands (pyridine and TBPO/TBP) have larger photoconductance at low fields than QDs passivated with longer chain ligands (TOPO and octanethiol). The results for overcoated QD solids also show the effect of increasing edge-to-edge separation of the CdSe cores. Overcoated samples consist of a CdSe core, with a shell of a second, larger band gap semiconductor. Table I shows that core-shell QDs have higher PL QY than bare QDs, but the overcoated QD solids are less photoconductive.

Figure 7 shows the results of simultaneous measurements of the band edge PL QY and the magnitude of the photocurrent as a function of applied electric field for a solid of 24 Å radius, TOPO/TOP passivated QDs. The decrease in the magnitude of the integrated PL intensity, $[\Phi(0)-\Phi(F)]/\Phi(0)$, with applied field (inset of Fig. 7) has a characteristic ''*W*'' shape reaching a maximum of 6% in an applied field of 150 kV/cm. In some samples, the dip observed near $\pm$50 kV/cm is so large that the PL QY may become slightly larger than the zero field PL QY before it decreases again. In other words, the field appears to enhance the PL at low fields but quenches it at high fields. No electroluminescence in the dark has been observed for either type of sample. The PL of single QDs, well dispersed on a quartz substrate so that there can be no charge transport, is reduced by less than 0.1% for applied fields of up to 10^5 V/cm. The band edge PL shows no Stark shift or broadening that might accompany changes in the radiative rate. Therefore, the PL quenching observed with the QD solid must be due to separation of excitons and not due to changes in the radiative or

TABLE I. Effect of surface passivation on the charge generation efficiency of 20 Å QD solids at 10 K.

Surface passivation	CdSe edge spacing (Å)	PL QY (%)	Charges per photon @ 250 kV/cm
TOPO/TOP	11±1	2	8*E*-5
Octanethiol	9±2	0.85	5.9*E*-5
TBPO/TBP	7±1	1	1.4*E*-5
Pyridine	7±1	~0.01	8.3*E*-6
3 monolayers CdS +TOPO/TOP	~31	24	<5*E*-6
3 monolayers ZnS +pyridine	~26	7	<5*E*-8

nonradiative rates of recombination. In samples with poor surface passivation, ''deep trap'' PL is observed far to the red of the band edge (Fig. 8). At 10 K, quenching of the deep trap PL is observed before quenching of the band edge emission is detectable (inset of Fig. 8).

The trends described in this section are reproducible and have been repeated several times with different sample series. The absolute magnitude of the photocurrent, however, may vary by as much as a factor of two for the same nominal sample preparation. Variations in sample thickness, degree of excess cap, as well as the macroscopic defect density in the films may contribute to this variability.

IV. DISCUSSION

A. Theoretical overview

The increase in conductivity ($\Delta\sigma$) of a material under steady state illumination is generally given by

$$\Delta\sigma = e(\Delta n \mu_n + \Delta p \mu_p), \tag{1}$$

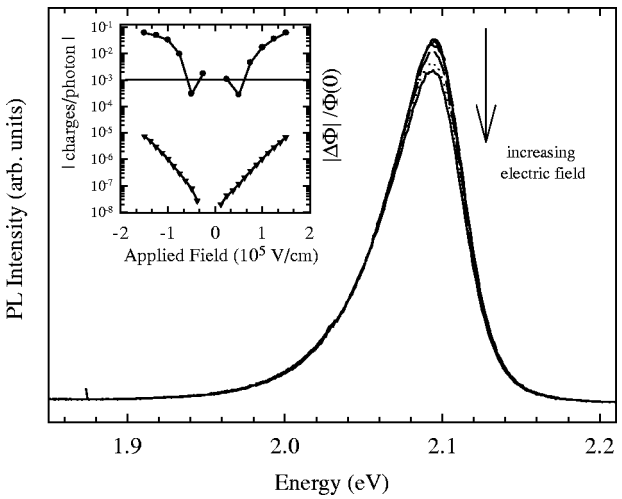

FIG. 7. Fluorescence quenching at 10 K for a well-passivated 24 Å TOPO/TOP capped QD solid. Spectra are taken in steps of 2.5×10^4 V/cm starting at 0 V/cm. In the inset, the fractional change in integrated PL intensity $-|\Delta\Phi|/\Phi(0)$ (●) and measured photocurrent (▼) in units of absolute charges per absorbed photon (the external efficiency) are plotted on the same scale. The thin line at 10^{-3} indicates the maximum fluorescence quenching of a single isolated QD in a similar electric field.

where Δn and Δp are the densities of photogenerated electrons and holes respectively and μ_n and μ_p are the respective mobilities. Both the density of free carriers and the mobility may depend on the applied electric field. In insulators, conducting polymers,[35] molecular solids[36] and other low mobility materials, the density of free carriers is often strongly field dependent and limited by the rate of geminate recombination of the photoexcited electron-hole pairs. In systems where the rate of intra-band relaxation is much faster than the rate of charge separation, the charge generation efficiency (number of free carriers/absorbed photon) depends on the branching ratio between the rate of geminate recombination and the rate of charge separation as[37]

$$\eta(F,T) = \frac{k_F(F,T)}{k_F(F,T) + k_r(T) + k_{nr}(T)}. \tag{2}$$

In Eq. (2), geminate recombination is expressed as the sum of k_r and k_{nr} (assumed to be weakly field dependent), k_F is the rate of charge separation under the applied electric field, and T is the sample temperature. The field dependence in η originates from the rate of charge separation.

In Secs. IV B through IV E we show that for QD solids, the strong field dependence of the photocurrent, the correlation between the temperature dependence of the photocurrent

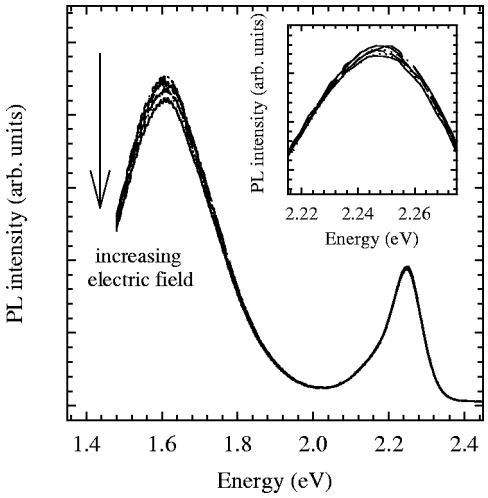

FIG. 8. Fluorescence quenching at 10 K for a poorly passivated 19 Å TOPO/TOP capped QD solid. The inset shows a blowup of the band edge PL. Quenching of the deep trap luminescence is observed before any quenching of the band edge PL is detectable.

and the exciton lifetime, and the correlation between the PL quenching and the photocurrent amplitude are all consistent with the model described by Eq. (2). Throughout the discussion we assume that each QD is never more than singly charged because of the large Coulomb charging energy (measured to be at least ~150 meV for 4–5 nm diameter CdSe QDs above a conducting substrate).[38] Since the charging energy is much larger than the available thermal energy at room temperature, each QD will never be more than singly charged until the entire QD array has been filled.

B. Temperature dependence

When limited by geminate recombination, the yield of carriers is strongly affected by the exciton lifetime. If the rate of geminate recombination is much greater than the rate of charge separation, Eq. (2) can be factored so that $\eta(F,T) = \tau(T)k_F(F)$ where $\tau(T)$ is the exciton lifetime $(1/\tau = k_r + k_{nr})$. The I-V characteristics in Fig. 3(a) are well described by the product of a field dependent function $\mathfrak{f}(F)$ that gives the shape of the I-V characteristic [Fig. 3(b)] and a temperature dependent function, $S(T)$ that controls the amplitude of the I-V curve. Figure 4 shows that $1/S(T)$ is similar in shape to both $\tau(T)$ and the PL QY(T) in the absence of an applied field. Similar QY(T) behavior has been observed in a number of TOPO/TOP capped samples making us confident that the similarity between $1/S(T)$ and the QY(T) is not merely fortunate coincidence. Both τ and the QY decrease with increasing temperature consistent with an increase in the nonradiative recombination rate within the parent QD.[39]

If we tentatively assign $1/S(T)$ to the exciton lifetime then the shape of the I-V characteristic must be related to the field dependent charge separation rate. In Fig. 3(b) $\mathfrak{f}(F)$ is nearly temperature independent suggesting that charge separation proceeds via tunneling. A tunneling mechanism is consistent with the large barriers that confine the electron and hole to the QD. In optical absorption measurements, only a small red shift (~2 nm) of the QD linear absorption spectrum is observed from dilute solution to close-packed films.[14] A large red shift would be expected if the electron or hole wavefunctions had significant leakage through the potential barrier. The binding energy of the quantum-confined exciton (~200 meV for a 20 Å QD) is also much greater than the available thermal energy at room temperature. Thus, one would not expect thermally assisted ionization of excitons to contribute significantly to the photocurrent.

A large number of samples show I-V characteristics that are well described by $\mathfrak{f}(F)\tau(T)$ and are consistent with tunneling between QDs. In a few cases however, the shape of the I-V characteristic is weakly temperature dependent and the photocurrent at low applied fields increases slightly with increasing temperature [see Fig. 3(c)]. If k_F is comparable to the exciton recombination rate $(k_r + k_{nr})$ then it is not possible to factor the expression for η, and a weakly temperature dependent I-V characteristic might be observed. However, the carrier yield should also be substantially increased compared to that for samples like the one in Figs. 3(a) and 3(b), leading to larger photocurrents. This is not observed. Similarly, if the mobility of free carriers was thermally activated, increased photocurrent would be expected. No correlation between the magnitude of the photocurrent and the temperature dependent behavior has been found for different samples, ruling out both these possibilities.

Weak temperature dependence without an increase in charge generation efficiency could be explained by thermal population of various QD surface defect states. In CdSe QDs, the deep trap PL (believed to be surface related) has been observed to increase between 10 and ~80 K before rapidly decreasing again.[40] We show evidence in Sec. IV C that charge separation of surface trapped carriers occurs at lower energy than separation of carriers confined to the core of the QD. Thermal population of surface defect states may increase the number of charges that escape from the QD via this low energy pathway. At the same time, defect states may also act as centers for nonradiative exciton recombination. Thus, the net yield of carriers may not be increased even though charge separation may be possible at lower applied fields.

C. Fluorescence quenching

Charge separation decreases the PL QY of charge neutral QDs by providing an additional nonradiative pathway for destruction of the excitons. A classic test for geminate recombination limited photoconductivity is that the charge separation efficiency derived from the magnitude of fluorescence quenching and the number of charges per absorbed photon collected at the electrodes are proportional. In QD solids (Fig. 7), we show that the photoconductive gain and the quenching of the band edge PL both change by approximately 2 orders of magnitude over the experimental range of applied fields. They are also both strongly field-dependent and have nearly the same shape at high fields, consistent with a geminate recombination limited system.

In many systems, the decrease in PL QY can be used as a direct, quantitative probe of the internal charge separation efficiency, independent of mobility and carrier lifetime effects.[37] This is not the case if the presence of free carriers introduces new nonradiative pathways for exciton annihilation. Efficient Auger-like nonradiative recombination where the exciton energy is transferred to a third carrier is believed to make charged QDs essentially ''dark'' in emission compared to neutral QDs.[41,42] In this model, the PL efficiency of the QD solid should be inversely proportional to the density of charge carriers in the QD solids since each exciton ionization event creates two charged QDs. Auger recombination may also be more efficient in QDs where the charge occupies a delocalized QD core electronic state rather than a localized trap state. The total PL quenching may thus depend on the rate of charge separation, the charge density within the QD solid, and the fraction of charged QDs where the charge is delocalized over the QD core.

Without an independent measure of the carrier density, we cannot directly extract the charge separation rate from the fluorescence quenching data. However, we can still make some qualitative observations about the charge separation process. In order to observe significant PL quenching (>1%), either the rate of charge separation is comparable to the radiative and nonradiative recombination rates or there is a non-negligible, field dependent density of charged QDs in the sample. The first scenario can be ruled out from the small charge generation efficiency as discussed in the previous sec-

tion on temperature dependence. Thus, we are left with the conclusion that while charge separation is a relatively slow process, there must be a significant charge density within the sample that quenches the PL. The characteristic ''*W*'' shape of the PL quenching data suggests that the charge density is initially decreased by the applied field and then increases again as the field is increased further. More experiments are required to understand this unusual behavior.

The band edge PL in CdSe QDs was recently assigned to recombination of electrons and holes in spherically symmetric QD core electronic states.[43] Work by Lifshitz *et al.* suggests that low energy broad ''deep trap'' PL originates from the recombination of shallow trapped electrons and deep trapped holes.[40] In Fig. 8 quenching of the deep trap PL is observed at lower fields than quenching of the band edge PL. This suggests that it is harder to separate excitons confined to the core of the QD than electron-hole pairs where one or both carriers are separately trapped at the surface of the parent QD. The wave function overlap is greater for electron-hole pairs delocalized in the core of the QD than for carriers localized in surface trap states. Consequently, the energy required to overcome the Coulomb attraction should be greater for the electron-hole pairs strictly confined to the core. This is discussed further in section F and in the calculations of Appendix A.

D. Intensity dependence

The intensity dependence of the photocurrent provides information about both the photocarrier generation mechanism and the recombination mechanisms for free carriers. Figure 2 shows that the photocurrent in the QD solid varies linearly with intensity consistent with a single photon mechanism for electron-hole pair generation and dissociation. Linear intensity further implies that either there is no recombination in the bulk of the sample, or that recombination is first order with respect to the concentration of free majority carriers (quasi-monomolecular recombination).

We eliminate the first possibility by considering the dependence of the absolute photocurrent on electrode spacing for fixed electric field and photon flux. If there is no carrier recombination in the bulk of the sample and the carrier mobility remains the same, then the total number of charge carriers between the electrodes should increase with increasing electrode spacing. Within our sample-to-sample reproducibility, we observe no dependence of the magnitude of the photocurrent on electrode spacing, for gaps between 1 and 20 μm, suggesting the photocurrent is not transit time limited.

In a trap-free insulator where the number of thermally generated carriers is much less than the number of photogenerated carriers, a square root dependence on intensity is expected from bimolecular recombination of the photogenerated electrons and holes.[44] First-order recombination kinetics can predominate if there are many more recombination centers than there are *free* majority carriers.[44] Optical studies have suggested that there are deep hole traps and shallow electron traps at the surface of colloidal QDs.[40] The deep hole traps could both limit hole mobility and act as recombination centers when filled. Shallow electron traps could limit the free electron concentration such that monomolecular recombination kinetics could predominate. While the properties of the QD solid are qualitatively consistent with this model, further measurements of the photoresponse time as a function of excitation intensity and temperature are required to confirm the presence and chemical nature of traps in the QD solid.

E. Field dependence

In this section we argue that the primary action of the electric field is to overcome the Coulomb attraction of the initial electron-hole pair and not to significantly lower the confinement barrier. The maximum potential dropped across two adjacent QDs in any of the experiments is only $\sim$0.25 eV—much less the potential that must confine the electron and to the QD. Instead the electric field brings an unoccupied state into resonance with the QD containing the exciton so that one of the charges can escape. Figure 5 shows that the curvature of the I-V characteristic increases with decreasing QD radius, consistent with an increase in the energy required to overcome the binding energy of the photogenerated electron-hole pair.

The dependence of the photocurrent on surface passivation and interparticle spacing (shown in Fig. 6 and Table I) suggest that these parameters affect the rate of charge separation. For example, the probability to tunnel through alkane ligands is proportional to $e^{-\alpha d}$ where $\alpha \sim 1$ Å^{-1}.[11] Thus if the density of states remains the same on changing the surface ligand from TOPO to TBPO, one would expect approximately a 42$\times$ increase in tunneling probability ($d_{\mathrm{TBPO}} \sim 7$ Å, $d_{\mathrm{TOPO}} \sim 11$ Å). In Fig. 6, we observe an approximately 10$\times$ increase in tunneling probability at low fields. A distribution of tunneling distances would make the tunneling probability less sensitive to the average interparticle spacing than expected from the simple theory.

The carrier generation efficiencies with core-shell QDs are also in qualitative agreement carriers tunneling out of the QDs. For QDs overcoated with 3 monolayers of ZnS ($\sim$3.1 Å per monolayer, conduction band offset $\sim$0.9 eV) and then capped with pyridine ligands ($d \sim 7$ Å), we observe that the charge generation efficiency is at least 1000$\times$ smaller than for bare TOPO capped QDs. For CdS overcoated QDs, where the CdS conduction band is nearly matched to the CdSe conduction band (offset $\sim$0.2 eV), we observe that the charge generation efficiency is only 16$\times$ smaller than for bare TOPO capped QDs. The observations for the core-shell QDs are consistent with findings in polymer QD composite LED's where improved efficiencies were observed with CdS overcoated QDs (Ref. 45) in comparison to ZnS overcoated particles.[46]

F. Tunneling model for charge generation

Geminate recombination systems have customarily been treated using the formalism developed by Onsager[47] and extended by a number of others.[37,48,49] In the simple Onsager model, the probability of geminate recombination depends on the Coulomb energy of the initially thermalized electron-hole pair compared to the strength of the applied electric field. While this qualitative picture is applicable to QD solids, none of these Onsager-type models account for cases where the Coulomb energy of the initial ion pair is much greater than the available thermal energy. At 10 K, the bind-

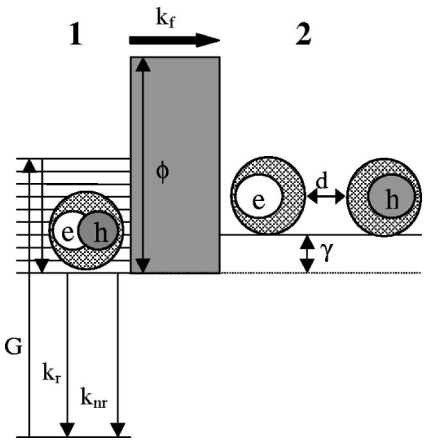

FIG. 9. Cartoon of the energy cost required to separate the initial electron-hole pair. γ is the energy cost, ''*d*'' is the distance between adjacent QDs, and ϕ is the potential barrier which confines the electron or hole to the QD. ϕ is related to the energy difference between the lowest conduction (valence) band state for the electron (hole) and the LUMO (HOMO) for the organic capping layer. See text.

ing energy of the confined exciton is much greater than *kT*; therefore within the Onsager model, the probability of charge escape is negligible except at extremely high fields. To model the field response of the photocurrent, we develop a simple two-site resonant tunneling model to account for the essential physics in the initial separation of the exciton. The calculations that follow provide intuition on how the shape of the *I-V* response should vary with changes in the experimental parameters.

Figure 9 summarizes the tunneling model in a simple cartoon. A quantum-confined exciton is created with generation rate *G* by absorption of a photon with energy greater than the band gap. This exciton rapidly relaxes to the lowest excited state of the QD where it can undergo radiative recombination, non-radiative recombination or ionization to create two adjacent, charged QDs. The probability that one charge escape depends on the height (ϕ) and width of the tunnel barrier (d) as well as the energy offset (γ) between the initial and final state. Increasing k_{nr} or k_r decreases the probability that one of the carriers escapes the parent QD. A two-site nearest neighbor tunneling model is sufficient to describe the essential physics because the intersite spacing is almost 2 orders of magnitude larger than in molecular systems. As a result, the probability for a charge to tunnel or hop more than one site away from its initial site in a single step is negligible.

We consider two possible mechanisms for a charge escaping from the QD (Fig. 10). In the first case that shall be referred to as ''core-to-core,'' both the electron and hole are in spherically symmetric, ''particle-in-a-sphere'' states. One charge tunnels directly into another spherically symmetric state in the adjacent QD. In the second case referred to as ''trap-to-trap,'' both charges are in trap states at the surface of the particle. One charge then tunnels into a trap state at the surface of the adjacent QD. In both cases, the energy cost for charge separation arises from the energy required to overcome the Coulomb interaction of the photoexcited electron-hole pair and the interaction of each charge with its respective image charges.

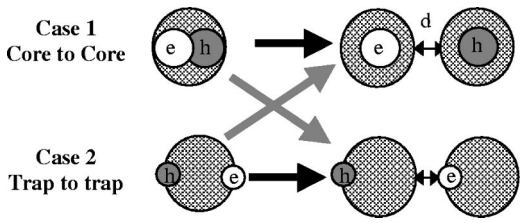

FIG. 10. Cartoon of the possible mechanisms for charge separation in QD solids. In case 1, charges tunnel directly between delocalized states. In case 2, the electron and hole are trapped on separate surface sites and one charge tunnels to the surface of an adjacent QD. Combinations of these mechanisms are also possible as indicated by the center arrows.

The details of how the net energy cost is calculated are given in Appendix A. Figure 11(a) shows the net energy cost as a function of QD size and interparticle spacing for core-to-core and trap-to-trap tunneling. Consistent with the data in Figs. 7 and 8, the energy cost to ionize the exciton decreases with increasing QD size and decreasing inter-particle spacing. The model predicts that tunneling from traps is a much lower energy process than tunneling directly from core electronic states and that the size dependence is relatively weak. Figure 11(b) shows the potential energy as a function of applied field in terms of the number of sites away from the parent QD. Once sufficient field is applied that one charge can move one site away from the parent QD, the probability to move further away is much greater than the probability to move back and carriers are swept by the electric field through the solid.

To fit the experimental *I-V* curves and extract an experimental value for γ, we model the transition rate (k) between

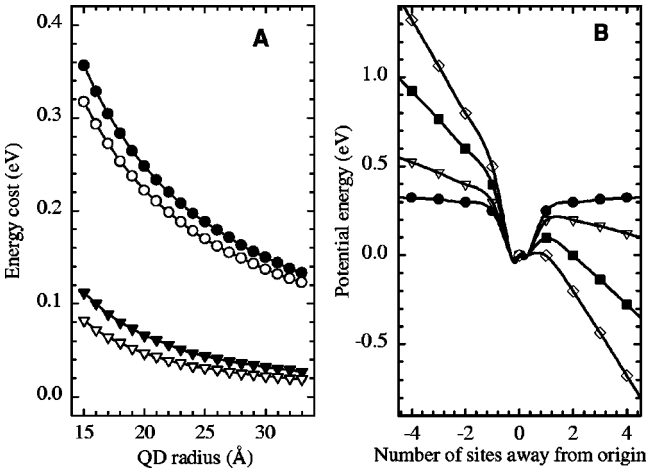

FIG. 11. (a) Calculated energy cost to separate electron-hole pairs confined to the core (circles) and trapped on the surface (triangles) as a function of QD radius. Closed symbols are for 11 Å spacings and open circles are for 7 Å spacing. (b) Calculated potential energy, relative to the energy of the bound exciton, as a function of the number of sites between the electron and hole in a QD solid with 11 Å interparticle spacing and 20 Å QDS. Symbols are for applied site to site energies of 0 meV (●), 50 meV (▽), 150 meV (◇), and 250 (■) meV.

state 1 and 2 using a golden rule approximation. Appendix B gives the details of the calculations used to develop the model. The three fitting parameters are the energy difference between the initial and final states (γ), the tunnel barrier height (ϕ) and a phenomenological parameter ''a'' that describes the amount of tailing of the density of states into the energy gap. The final result used to fit the data is the following:

$$I(\nu)=\frac{\exp\left(\frac{-4\sqrt{2}\hbar^2 d}{3m(e\nu-\gamma)}\left[\left(\frac{m\phi}{\hbar^2}\right)^{3/2}-\left(\frac{m(\phi+\gamma-e\nu)}{\hbar^2}\right)^{3/2}\right]\right)}{1+\exp\left(-\frac{\gamma-e\nu}{a}\right)}, \tag{3}$$

where ν is the *site-to-site* potential. Figure 12 shows the calculated I-v curves based on this tunneling model for two different inter-particle separations. The data is scaled on to the site-to-site potential by dividing the applied voltage by the approximate number of QDs between the electrodes. This assumes that the potential is dropped uniformly across the sample. The width of the tunnel barrier is fixed at the measured edge-to-edge spacing between the QDs. The value of γ is allowed to vary but the ratio of the energy cost for the TOPO vs TBPO (1.14 to 1) is fixed at the approximate ratio calculated from Eqs. (A2a) and (A2b) in Appendix A. A single tailing parameter ''a'' and barrier height (0.84 eV) are chosen to best fit all the data. The barrier height is chosen to give the same change in transmission probability as a function of alkane chain length as has been reported for dark conductivity measurements on close-packed gold nanoparticles.[11] For the scaled data the goodness of fit is sensitive to ''a'' and γ but is relatively insensitive to the value of ϕ.

The model qualitatively reproduces the field dependence of the photocurrent. For the best fit, the values of γ are intermediate between the trap-to-trap and the core-to-core limits ($\sim$150 meV). The intermediate value for γ may suggest that both pathways are active in the QD solids. The slight sample-to-sample variation observed might be due to variations in the degree of surface passivation or oxidation that may shift the balance between core-to-core and trap-to-trap tunneling. Quantitatively there are some problems with the model. For example, the escape rate (k_F) predicted from the fit parameters is much too large: If the attempt frequency for a charge to escape from the QD is approximately proportional to the orbital frequency ($\sim 10^{13}$ Hz), and the average transmission probability for a 0.84 eV barrier is $\sim 10^{-4}$, then for TOPO capped particles, this yields a value for k_F of $10^9\ s^{-1}$. Using Eq. (2) this implies efficiencies of nearly 100% (given 25 ns lifetime at 10 K). This value is too high compared to what is observed in Fig. 7 ($<$6%). Better agreement with the observed photoconductive gain is found if the height of the tunnel barrier is increased. However, then the absolute value of the photocurrent is predicted to be much more sensitive to the inter-particle spacing (d) than is observed. Part of the difficulty may arise since the WKB model assumes a continuum of states above the barrier that is inappropriate for a molecular tunnel barrier. To compensate for the low density of states for the molecular tunnel barrier, the apparent barrier height may need to be smaller. Alternatively, the difficulty in producing a unique fit may arise from the complementary nature of the ''a'' and ϕ parameters. A large tunnel barrier height can be somewhat compensated for by increasing the ''a'' parameter to increase the density of available states at low energy.

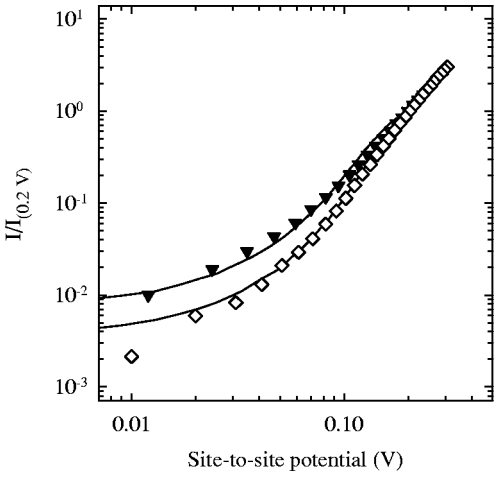

FIG. 12. Comparison between the data (symbols) and the tunneling model (lines) at 10 K. Data is for 20 Å QDs with ($\diamond$) TOPO ($d\sim 11$ Å, γ=0.170) and ($\blacktriangledown$) TBPO ($d\sim 7$ Å, γ=0.150) surface ligands. In the model, ϕ is fixed at 0.84 eV, and ''a'' is fixed at 0.060.

Without an independent measure of either the density of states or the energy levels in the organic molecules with respect to the ''conduction band'' and ''valence band'' edges of the QD, more quantitative analysis is not possible. The primary utility of the model is to provide intuition on how the shape of the I-V curve should vary with changes in experimental parameters. For example, decreasing interparticle spacing or increasing the QD size gives rise to I-V curves that are more linear and more photoconductive at low fields (see Figs. 5 and 6). Reducing the number of intermediate trap states, for example by overcoating the QDs, should promote core-to-core tunneling, a pathway leading to highly nonlinear I-V curves and low photoconductivity except at high applied electric fields. Consistent with the model, Table I shows that very little photoconductivity is observed with the overcoated QDs compared to the nonovercoated samples. The model also predicts that ligands that act as shallow traps for one carrier and not the other promote initial charge separation of the exciton leading to higher efficiency and weaker

field dependence. Recent intraband relaxation measurements suggest pyridine acts as a good hole acceptor[50,51] and would therefore promote the separation of electron-hole pairs and enhance the charge separation efficiency. Table I also shows that pyridine capped QDs exhibit low PL efficiency but moderate photoconductivity compared to TOPO capped QDs. While pyridine may promote charge separation, the low PL QY of pyridine capped QDs suggests that that this ligand also increases nonradiative recombination, thereby reducing the net carrier yield.

G. Final comments

Semiconductor QD solids present a unique opportunity to study the dynamics of charge separation in systems where the initial separation of the electron-hole pair can be well controlled. The calculations in Sec. IV F show the importance of the relative dielectric constant of the QD versus the surrounding matrix for nanometer scale systems as well as the importance of interface states. The large dielectric contrast of the semiconductor core versus the organic ligands leads to a large polarization energy that increases the energy cost to separate the photoexcited electron-hole pair.

Despite the success of the simple model presented in qualitatively describing the charge separation process, it is clear that many theoretical challenges remain to develop a complete description. In particular it is not clear where the applied potential is dropped, i.e., across the QD or across the organic. The calculations of the Coulomb interaction of charges on adjacent QDs are nontrivial and may need to be addressed using numerical methods. Finally, a more complete description of the potential energy near the interface and the relative positions of the HOMO and LUMO for the organic molecules *bound* to the surface of the QD are required for quantitative evaluation of the tunneling probability.

V. CONCLUSIONS

Photoconductivity in QD solids is the result of field assisted ionization of a photoexcited exciton in its lowest excited state. Charge separation competes with rapid radiative and non-radiative recombination which both act to decrease the internal charge generation efficiency. Charge separation proceeds primarily via a tunneling process and the field dependence of the photocurrent depends on the energy required to separate the electron-hole pair. A resonant tunneling model for charge separation qualitatively reproduces the QD size and surface passivation dependence of the photocurrent. Regardless of whether charges escape from trap states or from QD core electronic states, the energy required for charge separation is considerably larger than the available thermal energy, even at room temperature. It is clear that carrier access to the surface of the QD can improve the charge separation efficiency provided the surface does not also present sites for non-radiative recombination. The precise mechanism underlying the fluorescence quenching is not understood at this time. It may be related to the density of charges (both free and trapped) in the QD solid. The intensity dependence of the photocurrent indicates there is carrier recombination in the sample that reduces the external efficiency.

ACKNOWLEDGMENTS

Device fabrication was performed at the M.I.T. Center for Materials Science microfabrication lab and the Microsystems Technology Laboratory. C.A.L., N.Y.M. and S.A.E. would like to thank NSERC-Canada, the Lucent Technologies GRPW, and the Lester Wolfe Foundation, respectively, for financial support. We thank the M.I.T. Harrison Spectroscopy Laboratory (NSF-CHE-97-08265) for use of its facilities. This work was supported primarily by the MRSEC Program of the National Science Foundation under Grant No. DMR 98-08941.

APPENDIX A

Generally, the energy cost for charge separation can be written as the difference between E_2 and E_1

$$E_1 = E_c + E_p + E_{se} + E_{sh}, \tag{A1a}$$

$$E_2 = E_{\mathrm{Coul}} + E'_{se} + E'_{sh}, \tag{A1b}$$

where E_c is the direct Coulomb interaction between the electron and hole, E_p is the polarization energy arising from the interaction between the each carrier and the image charge of the other carrier, and the electron and hole self-charging energies are E_{se} and E_{sh}, respectively. E_1 is commonly known as the exciton binding energy. In E_2, the Coulomb interaction between charges in adjacent QDs (E_{Coul}) is approximated by the interaction energy of two point charges in a medium of average dielectric constant ($\varepsilon_{\mathrm{ave}} \sim 3\varepsilon_0$).[52] We neglect the interaction of each carrier with the image charge of the other carrier when the charges are in adjacent QDs.

For the case of core-to-core tunneling, each charge is assumed to be in a spherically symmetric state and the energy cost ($\gamma = E_2 - E_1$) can be derived using the results of Brus[53,54] and Babic:[55]

$$E_1 = \frac{-1.79q^2}{4\pi\varepsilon_0\varepsilon_{\mathrm{QD}}R} + \frac{q^2}{4\pi\varepsilon_0}\left(\frac{1}{\varepsilon_{\mathrm{QD}}} - \frac{1}{\varepsilon_{\mathrm{ave}}}\right) + 2\frac{q^2}{2\varepsilon_{\mathrm{QD}}R}S_s, \tag{A2a}$$

$$E_2 = -\frac{-q^2}{4\pi\varepsilon_0\varepsilon_{\mathrm{ave}}(2R+d)} + 2\frac{q^2}{2\varepsilon_{\mathrm{QD}}R}S_s, \tag{A2b}$$

where

$$S_s = 2\pi^2 \sum_{l=0}^{\infty} \frac{(l+1)(\varepsilon_{\mathrm{QD}} - \varepsilon_{\mathrm{ave}})}{(\varepsilon_{\mathrm{ave}} + l(\varepsilon_{\mathrm{ave}} + \varepsilon_{\mathrm{QD}}))} \int_0^1 \left(\frac{\sin(\pi x)}{\pi x}\right)^2 x^{2l+2} dx.$$

In Eqs. (A2a) and (A2b), $\varepsilon_{\mathrm{QD}}$ is the bulk, high frequency dielectric constant for CdSe ($6.2\varepsilon_0$) (Ref. 56) and R is the radius of the QD. It is assumed that the quantum confinement energy is the same in both E_1 and E_2 (valid within the strong confinement regime) as well as the self-charging energies for electron and hole. The latter approximation means that the self-charging energies will cancel in the expression for γ. The expression for E_2 is approximate and should be considered an upper bound only. A correct calculation of the interaction energy of two delocalized charge distributions at such short range requires a quantum mechanical calculation that is beyond the scope of this work.

For the case of trap-to-trap tunneling, the situation is somewhat simpler since the electron and hole can be treated as localized point charges. If trapped charges are localized on unpassivated Cd or Se atoms on opposite sides of the QD, the energy for charge separation is given using the results of Shim *et al.*:[57]

$$E_1=\frac{-q^2}{8\pi\varepsilon_0\varepsilon_{\mathrm{QD}}r}+\sum_{l=0}^{\infty}\frac{q^2}{2\pi\varepsilon_0\varepsilon_{\mathrm{QD}}}\frac{(\varepsilon-1)(2l+2)r^{4l+2}}{[(\varepsilon+1)(2l+1)+1]R^{4l+3}}, \tag{A3a}$$

$$E_2=2\sum_{l=0}^{\infty}\frac{q^2(\varepsilon-1)(l+1)}{8\pi\varepsilon_0\varepsilon_{\mathrm{QD}}(\varepsilon l+l+1)R}\left(\frac{r}{R}\right)^{2l}-\frac{q^2}{4\pi\varepsilon_0\varepsilon_{\mathrm{ave}}(2R+d)}, \tag{A3b}$$

where is $\varepsilon=\varepsilon_{\mathrm{QD}}/\varepsilon_{\mathrm{ave}}$ and r is the radius of the semiconductor core including the surface, minus the ionic radius of the Se^{-2} ion (1.98 Å).[58] E_1 is the sum of the Coulomb interaction for two charges on opposite side of the QD plus the polarization energy for these two localized charges. E_2 is the self-charging energy for a singly charged dielectric sphere with a point charge near the surface[54] plus the Coulomb interaction with the point charge on the other sphere. γ in this case is a lower bound on the energy required for charge separation. If the static dielectric constants for the semiconductor and organic components are used (probably more appropriate for tunneling from localized states), the energy cost will be increased.

APPENDIX B

Using the golden rule approximation, the transition rate (k) between two states can be written as the following:

$$k\propto\int_{-\infty}^{\infty}T(E)g_1(E)g_2(E)[F_1(E)-F_2(E)]dE, \tag{B1}$$

where $T(E)$ is the transition probability through the barrier, $g(E)$ is the density of states, and $F(E)$ is the Fermi distribution function in state 1 or 2, respectively. Since all the experiments are at low temperature and low excitation intensity, Eq. (B1) can be approximated by assuming that only state 1 is initially occupied and there is no thermal population of higher excited states. For simplicity, the back transition rate is assumed to be zero. The energy in the initial state is held fixed at zero for all applied biases and only the energy of the final states is allowed to vary. Equation (B1) then simplifies to

$$k(\nu)\propto T(0,V)g_2(-\gamma+eV), \tag{B2}$$

where e is the elementary charge, γ is the energy in the final state at zero applied bias, and ''ν'' the potential difference between the centers of adjacent QDs (the site to site potential). For plane waves incident on a barrier of width (d), the transmission probability is given by the following (WKB approximation):

$$|T(E)|^2\approx\exp\left[-2\int_0^d\sqrt{\frac{2m}{\hbar^2}(\phi(x)-E)}dx\right]. \tag{B3}$$

We assume a square tunnel barrier of height ϕ_0. Applying a linear potential, the tunneling barrier is given by

$$\phi(x)=\phi_0-\frac{eV}{d}x. \tag{B4}$$

For high, narrow barriers, the transmission probability varies approximately linearly with applied voltage. For tunneling through organic ligands, we use ''m'' equal to the rest mass of the electron. The existence of a finite size distribution in the sample transforms the discrete density of states in the individual QDs into an effective continuum in the QD solid. We assume a continuum density of states of the form

$$g_2(E)=\frac{1}{1+\exp\left(\frac{-E+\gamma}{a}\right)}. \tag{B5}$$

The parameter ''a'' controls the amount of ''tailing'' into the energy gap. Physically a large value for ''a'' means that there is a high density of trap states or a broad distribution of QD sizes and interparticle spacings in the sample. This functional form for the density of states is only valid for applied fields less than γ; in the real system the density of states should continue to increase with increasing energy.

*Present address: IBM, T. J. Watson Research Center, P.O. Box 218, Route 134, Yorktown Heights, NY 10598.

†Present address: Quantum Dot Corp., 4030 Fabian Way, Palo Alto, CA 94303.

‡Author to whom correspondence should be addressed: 77 Massachusetts Avenue, Room 6-223, Cambridge, MA 02139. Email: mgb@mit.edu

[1] L. Esaki and R. Tsu, IBM J. Res. Dev. **14**, 61 (1970).

[2] J. J. Welser, S. Tiwari, S. Rishton, K. Y. Lee, and Y. Lee, IEEE Electron Device Lett. **18**, 278 (1997).

[3] C. S. Lent, P. D. Tougaw, W. Prod, and G. H. Bernstein, Nanotechnology **4**, 49 (1993).

[4] W. Porod, C. S. Lent, G. H. Bernstein, A. O. Orlov, I. Amlani, G. L. Snider, and J. L. Merz, Int. J. Electron. **86**, 549 (1999).

[5] A. N. Korotkov, Int. J. Electron. **86**, 511 (1999).

[6] A. P. Alivisatos, Science **271**, 933 (1996).

[7] M. A. Kastner, Phys. Today **46**, 24 (1993).

[8] C. B. Murray, C. R. Kagan, and M. G. Bawendi, Science **270**, 1335 (1995).

[9] B. A. Korgel and D. Fitzmaurice, Phys. Rev. Lett. **80**, 3531 (1998).

[10] C. P. Collier, T. Vossmeyer, and J. R. Heath, Annu. Rev. Phys. Chem. **49**, 371 (1998).

[11] R. H. Terrill, T. A. Postlethwaite, C. H. Chen, C. Poon, A. Terzis, A. Chen, J. E. Hutchison, M. R. Clark, G. Wignall, J. D. Londono, R. Superfine, M. Falvo, C. S. Johnson, Jr., E. T. Samulski, and R. W. Murray, J. Am. Chem. Soc. **117**, 12 537 (1995).

[12] R. P. Andres, J. D. Bielefeld, J. I. Henderson, D. B. Janes, V. R.

Kolagunta, C. P. Kubiak, W. J. Mahoney, and R. G. Osifchin, Science **273**, 1690 (1996).
[13] C. P. Collier, R. J. Saykally, J. J. Shiang, S. E. Henrichs, and J. R. Heath, Science **277**, 1978 (1997).
[14] C. R. Kagan, C. B. Murray, and M. G. Bawendi, in *Microcrystalline and Nanocrystalline Semiconductors*, edited by L. Brus, M. Hirose, R. W. Collins, F. Koch, and C. C. Tsai, MRS Symposia Proceedings No. 358 (Materials Research Society, Boston, 1995), p. 219.
[15] C. R. Kagan, C. B. Murray, and M. G. Bawendi, Phys. Rev. B **54**, 8633 (1996).
[16] C. B. Whan, J. White, and T. P. Orlando, Appl. Phys. Lett. **68**, 2996 (1996).
[17] V. L. Colvin, M. C. Schlamp, and A. P. Alivisatos, Nature (London) **370**, 354 (1994).
[18] B. O. Dabbousi, M. G. Bawendi, O. Onitsuka, and M. F. Rubner, Appl. Phys. Lett. **66**, 1316 (1995).
[19] M. V. Artemyev, V. Sperling, and U. Woggon, J. Appl. Phys. **81**, 6975 (1997).
[20] Y. Wang and N. Herron, Chem. Phys. Lett. **200**, 71 (1992).
[21] Y. Wang and N. Herron, J. Lumin. **70**, 48 (1996).
[22] N. C. Greenham, X. G. Peng, and A. P. Alivisatos, Phys. Rev. B **54**, 17 628 (1996).
[23] D. S. Ginger and N. C. Greenham, J. Appl. Phys. **87**, 1361 (2000).
[24] C. B. Murray, D. J. Norris, and M. G. Bawendi, J. Am. Chem. Soc. **115**, 8706 (1993).
[25] M. Kuno, J. K. Lee, B. O. Dabbousi, F. V. Mikulec, and M. G. Bawendi, J. Chem. Phys. **106**, 9869 (1997).
[26] M. A. Hines and P. Guyot-Sionnest, J. Phys. Chem. **100**, 468 (1996).
[27] B. O. Dabbousi, J. RodriguezViejo, F. V. Mikulec, J. R. Heine, H. Mattoussi, R. Ober, K. F. Jensen, and M. G. Bawendi, J. Phys. Chem. B **101**, 9463 (1997).
[28] R. K. Iler, *The Chemistry of Silica* (Wiley, New York, 1979), p. 622.
[29] S. A. Empedocles, D. J. Norris, and M. G. Bawendi, Phys. Rev. Lett. **77**, 3873 (1996).
[30] For a detailed description of the electronic transitions that make up the linear optical absorption spectrum of CdSe QDs, see D. J. Norris and M. G. Bawendi, Phys. Rev. B **53**, 16 338 (1996).
[31] C. R. Kagan, Ph.D. thesis, Massachusetts Institute of Technology, Cambridge, 1996, p. 169.
[32] O. I. Micic, K. M. Jones, A. Cahill, and A. J. Nozik, J. Phys. Chem. B **102**, 9791 (1998).
[33] V. Klimov, P. H. Bolivar, and H. Kurz, Phys. Rev. B **53**, 1463 (1996).
[34] N. Y. Morgan, I. Prasad, C. A. Leatherdale, M. A. Kastner, and M. G. Bawendi (in preparation).
[35] S. Nespurek, V. Cimrova, J. Pfleger, and I. Kminek, Polym. Adv. Technol. **7**, 459 (1996).
[36] L. B. Lin, S. A. Jenekhe, and P. M. Borsenberger, J. Chem. Phys. **105**, 8490 (1996).
[37] J. Noolandi and K. M. Hong, J. Chem. Phys. **70**, 3230 (1979).
[38] B. Alperson, S. Cohen, I. Rubinstein, and G. Hodes, Phys. Rev. B **52**, R17017 (1995).
[39] The $QY(T)$ can be fit quite well to a Mott-Seitz form ($1/QY \propto 1 + Ae^{-\Delta E/kT}$) where $\Delta E \sim 12$ meV for QDs with TOPO/TOP ligands. While the lifetime and *QY* as a function of temperature appear to be dominated by the nonradiative rate, the radiative rate should also be temperature dependent. The lowest energy exciton state in CdSe QDs is believed to be optically dark (see Ref. 43) and thermal population of a nearby optically bright state should increase the radiative rate with increasing temperature.
[40] E. Lifshitz, I. Dag, I. Litvin, G. Hodes, S. Gorer, R. Reisfeld, M. Zelner, and H. Minti, Chem. Phys. Lett. **288**, 188 (1998).
[41] D. I. Chepic, A. L. Efros, A. I. Ekimov, M. G. Vanov, V. A. Kharchenko, I. A. Kudriavtsev, and T. V. Yazeva, J. Lumin. **47**, 113 (1990).
[42] The increased nonradiative rate is proposed to occur in an efficient Auger-like process where the exciton energy is transferred to the unpaired charge. The unpaired charge is excited to higher electronic states and then is ejected from the QD, or if the barrier is sufficient, simply thermalizes to the ground state. Chepic *et al.* (Ref. 41) postulated this effect to explain the observations that for semiconductor QDs embedded in glasses, strong illumination with light to the blue of the band edge caused photodarkening and a large increase in the nonradiative rate that was reversible upon heating. The photodarkening was attributed to ionization of the QDs (see V. J. Grabovskis *et al.*, Fiz Tverd. Tela (Leningrad) **31** (1989) [Sov. Phys. Solid State **31**, 272 (1989)]). Recently a similar effect was observed for dilute CdTe QDs in a TOPO matrix [M. Y. Shen *et al.*, Phys. Rev. Lett. **82**, 3195 (1999)].
[43] M. Nirmal, D. J. Norris, M. Kuno, M. G. Bawendi, A. L. Efros, and M. Rosen, Phys. Rev. Lett. **75**, 3728 (1995).
[44] R. H. Bube, *Photoconductivity of Solids* (Wiley, New York, 1960).
[45] M. C. Schlamp, X. G. Peng, and A. P. Alivisatos, J. Appl. Phys. **82**, 5837 (1997).
[46] H. Mattoussi, L. H. Radzilowski, B. O. Dabbousi, E. L. Thomas, M. G. Bawendi, and M. F. Rubner, J. Appl. Phys. **83**, 7965 (1998).
[47] L. Onsager, Phys. Rev. **54**, 554 (1938).
[48] S. Rackovsky and H. Scher, Phys. Rev. Lett. **52**, 453 (1984).
[49] Y. Wang and A. Suna, J. Phys. Chem. B **1997**, 5627 (1997).
[50] P. Guyot-Sionnest, M. Shim, C. Matranga, and M. Hines, Phys. Rev. B **60**, R2181 (1999).
[51] V. I. Klimov, A. A. Mikhailovsky, D. W. McBranch, C. A. Leatherdale, and M. G. Bawendi, Phys. Rev. B **61**, R13 349 (2000).
[52] The average dielectric constant of the QD solid is calculated for randomly close-packed spheres (fill factor=0.64) of semiconductor with an organic shell of width (*d*). The interstices are filled with the same organic material $\varepsilon \sim 2\varepsilon_0$.
[53] L. E. Brus, J. Chem. Phys. **80**, 4001 (1984).
[54] L. E. Brus, J. Chem. Phys. **79**, 5566 (1983).
[55] D. Babic, R. Tsu, and R. F. Greene, Phys. Rev. B **45**, 14 150 (1992).
[56] L. Wang and A. Zunger, Phys. Rev. B **53**, 9579 (1996).
[57] M. Shim and P. Guyot-Sionnest, J. Chem. Phys. **111**, 6955 (1999).
[58] The charge is placed slightly inside the boundary of the dielectric sphere in order to avoid the interface where the potential is undefined. The trapped charge is assumed to be on an unpassivated Se site. r=core radius+1.5 Å−Se^{-2} ionic radius. R=core radius+1.5 Å.